

X-ray spectral properties of nearby AGN using clumpy torus model.

Koushika VP¹, Corral A¹, Carrera FJ¹, Laloux B², and Akylas A², and Georgakakis A²

¹ Instituto de Física de Cantabria (CSIC- Universidad de Cantabria), Santander, Spain

² National Observatory of Athens, Athens, Greece

Abstract

We have used a sample of 50 nearby ($z \leq 0.06$) obscured and unobscured AGN (about half of each) with NuSTAR hard X-ray spectra to explore the capabilities of clumpy torus models that represent the wide variety of X-ray spectral properties shown by AGN. We have used UXCLUMPY, which allows self-consistent multi-wavelength analyses. We have found that good individual spectral fits can be obtained with that model for all sources, including Compton Thick sources. We were looking for the smallest set of model parameters, that fit reasonably well with all our sources. We found that 23 such model parameter combinations span the sample, and additionally, they can be grouped into only four basic spectral shapes. We will extend this approach to an expanded sample and use the resulting maximally spanning sets of model parameter combinations to simulate AGN observations with *Athena*, to develop a method for automatically determining redshifts from their X-ray spectra.

1 Introduction

The compact centers of some galaxies accrete matter and emit enormous amounts of radiation at all wavelengths. These are called active galactic nuclei (AGN) [20]. They are persistent sources across all redshifts of the observable Universe[4][11][24]. It is essential to understand these enigmatic objects to answer important questions about the environment of the early Universe, the growth of SMBH[1] [5], and the evolution of galaxies.[15] [17]

AGN models theorize the presence of a torus-shaped dusty region that encloses the central supermassive black hole (SMBH) and the accretion disk[16]. The material related to the torus would be responsible for the obscuration [8] seen along the lines of sight to many AGN, if not most. Several studies have pointed out from observational evidence that the nature of this obscuring structure is clumpy.[18][19]

X-rays are produced at regions close to the SMBH through thermal and non-thermal processes [21]. Thanks to their high penetrating power, X-rays could be used to probe the central

regions. Also, a part of the intrinsic UV/optical continuum radiation from the accretion disk gets reprocessed into X-rays by the geometric features present near the accretion disk[12]. This leaves an imprint on the X-ray continuum spectra with the characteristic emission lines. Thus, X-rays can not only be used to study the properties of the central SMBH but also to understand the anatomy of the AGNs and the physical processes in the inner regions that characterize a particular source[6]. One of the fundamental properties required to characterize the AGN is redshift (z). The redshift of an object not only tells us how far away it is but also its age and, in turn, its nature. This helps us understand the stages of evolution in the AGN life cycle.[10]

Our ultimate aim is to extract redshift information entirely from the X-ray spectrum of the AGN. A characteristic feature in the reflection X-ray spectrum of the AGN is the Fe K- α line [9]. It is produced when the continuum emission is reprocessed by the circumnuclear material. Thus, this line gives an important diagnosis of the nature of the AGN's surroundings[7] [13]. The redshift of the AGN can be found by identifying the energy at which this Fe K α line is present in the X-ray spectrum. Previous studies have attempted to do this characterization by employing a fitting method directly on the observed spectra and filtering techniques on simulated data [3][22][23].

In this work, we present preliminary results, representative AGN spectral shapes from the nearby AGN population. These will then be used for simulations in particular for *Athena*/WFI surveys which will be used for testing and optimizing our redshift extraction algorithm. Representative AGN spectral shapes are obtained using NuSTAR data from a nearby AGN population and a recent, up-to-date clumpy torus model. The data and the model are explained in section 2. Methodology, results, and conclusions are presented in Section 3, Section 4, and Section 5 respectively.

2 Sample data and model

2.1 Data

Our sample consists of 50 Seyfert objects, of which 29 are Seyfert Type-I and 21 are Seyfert Type-II. Out of 21 Type-II sources, 7 are Compton thick (CT; neutral hydrogen column density, $N_H \geq 1.5 \times 10^{24} \text{cm}^{-2}$) and 14 are Non-CT. The important obscuration features, the Fe K α line, and the Compton edge occur in the hard X-ray energy range. The Nuclear Spectroscopic Telescope Array, NuSTAR [14] operates between 3 and 79 keV and fits the criteria. NuSTAR data for our sample were extracted with the standard NuSTAR pipeline. The sample can be accessed in the link <https://doi.org/10.5281/zenodo.7390156>

2.2 Model

We have employed a recent and up-to-date clumpy torus model UXCLUMPY [2]. The model assumes a central X-ray source surrounded by an inner ring of Compton thick clouds and an outer ring of diffuse, Compton thin clouds. The model is self-consistent and reproduces the X-ray and IR spectra of nearby AGN. The model parameters are explained in Table 1

Table 1: UXCLUMPY Model Parameters

Parameter	Description	Range	Bins in the Table model
NH (N_H)	Total LOS column density [cm^{-2}]	$10^{20} - 10^{26}$	41 bins
PhoIndex (Γ)	Photon index	1-3	11 bins
Ecut (E_{cut})	Energy cut-off [keV]	60-400	60, 100, 140, 200, 400
TORsigma (σ)	Vertical cloud dispersion	0-84°	0°, 7°, 28°, 84°
CTKcover (C)	Covering fraction of inner CT ring	0-0.6	0, 0.25, 0.3, 0.45, 0.6
Theta_inc (θ_{inc})	Viewing angle	0-90°	0°, 60°, 90°

3 Methodology

In a holistic approach, data from the NuSTAR FPMA module and Xspec model *atable{uxclumpy-cutoff.fits} + atable{uxclumpy-cutoff-omni.fits} *const* were used. The *const* parameter defines the fraction of the total intrinsic component that is scattered. All the parameter values were fixed from the values of the parameter combinations from the UXCLUMPY table model.

1. Each of the sources is fitted with parameter combinations allowing only *normalization* and *const* parameters to vary
2. For each fit, χ^2 statistic and degrees of freedom (dof) are noted
3. For each parameter combination, global χ^2/dof ¹ - contribution of χ^2/dof from each source fit is calculated
4. The parameter combinations are then arranged in a table in the increasing order of the global χ^2/dof
5. When the individual $\chi^2/\text{dof} \leq 1.5$ for a fit, the particular parameter combination is said to have spanned that object
6. Starting from the parameter combination with the least global χ^2/dof in the rearranged table, a new one is included only if it adds to the spanned list a new object

4 Results and Discussions

Following the method established earlier, we obtained 23 models in Table 2 that span the entire sample.

¹Global χ^2/dof is a measure of how well a parameter combination fits all the objects of the sample set. This includes both $\chi^2/\text{dof} \leq 1.5$ for objects that it fits well and χ^2/dof for the objects that it does not. For example, this quantity tells the parameter combination 1 in the table in addition to fitting very well 26 objects, it has fitted fairly-well other objects in comparison to the parameter combination 2

Table 2: 23 Models that are required to span the sample set

	N_H	Γ	E_{cut}	σ	C	θ_{inc}	$const_{avg}$	global	Number of Objects spanned			
	$10^{22} cm^{-2}$			deg		deg		χ^2/dof	Total	Sy1	Non CT	CT
1	1.78	1.8	100	84	0	60	0.04	3.47	26	19	7	0
2	1.26	1.8	100	84	0	60	0.04	3.48	28	21	7	0
3	1.26	1.8	100	84	0.25	90	0.04	3.51	29	22	7	0
4	1.26	1.8	100	28	0	60	0.04	3.52	27	20	7	0
5	2.51	2	400	84	0.25	90	0.05	3.56	25	18	7	0
6	3.55	1.8	200	7	0	90	0.08	3.59	23	16	7	0
7	3.55	1.8	140	84	0	90	0.02	3.91	17	10	7	0
8	1.26	2	140	84	0.3	60	0.09	4.10	21	15	6	0
9	0.891	2	140	84	0.25	0	0.09	4.35	20	14	6	0
10	7.08	1.8	140	7	0.25	90	0.08	4.38	10	4	5	1
11	1.26	2	100	84	0.25	0	0.08	4.43	18	12	6	0
12	7.08	1.8	200	7	0	90	0.07	4.53	9	3	5	1
13	10	1.8	400	7	0.25	90	0.06	6.01	7	1	4	2
14	10	1.8	140	28	0	0	0.06	7.28	8	1	5	2
15	14.1	1.6	100	7	0.25	90	0.05	10.28	5	0	3	2
16	14.1	1.4	60	7	0	60	0.06	13.63	5	0	3	2
17	28.2	1.8	400	7	0.25	60	0.07	16.23	5	0	3	2
18	891	1.6	60	0	0.3	60	0.02	18.00	1	0	0	1
19	891	2	200	28	0	0	0.01	20.60	2	0	0	2
20	56.2	1.8	200	0	0.25	60	0.04	25.77	2	0	1	1
21	79.4	1.8	100	7	0	60	0.01	26.43	2	0	1	1
22	79.4	1.6	60	7	0	90	0.01	29.53	3	0	2	1
23	224	1.8	60	28	0	60	0.05	33.01	3	0	0	3

An example fit is shown in Figure 1 for an object NGC 424. The number of models required to span each category of objects is presented in Table 3. From the Table, it is clear that only a few different parameter combinations are required to span/represent the unabsorbed and the mildly absorbed population of sources. Also, only the first 11 parameter combinations are required to span $\sim 74\%$ of the sample which includes 100% of Type-I and 57% of the Type-II sources.

On the other hand, heavily absorbed sources practically require one combination each. This is attributed to the fact that as absorption increases, the underlying continuum power law diminishes and the signatures of the interesting complex absorbing material become more and more prominent.

Interestingly, these 23 parameter combinations can be grouped into 4 different groups based on the spectral shape they produce. The shape groups are represented in Figure 1. The groups clearly show the influence that the amount of absorption has in determining the

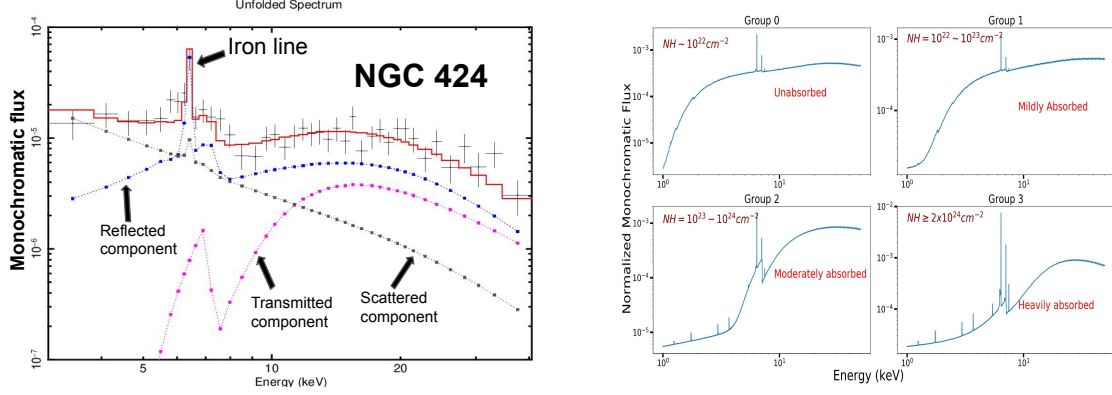


Figure 1: *Left*: Showing the model components of one fit. *Right*: Spectral shape groups into which the 23 parameter combinations can be grouped

Table 3: Models required to span each AGN type

Source Type	Number of Sources	Number of Parameter combinations required to span ^a
Sy1	29	9
Non CT Sy2	14	8
CT Sy2	7	7

^aFew parameter combinations are common in spanning Sy1s and Non CT Sy2s.

spectral shape of an object.

5 Conclusions and Future work

Using a representative sample, we obtained 23 representative AGN spectra. Type-I and mildly absorbed Type-II sources prefer similar spectral shapes. Moderately and heavily absorbed Type-II sources prefer to be more unique.

It is also noticed that parameter combinations with low to medium absorption span a range of objects simultaneously and prefer having a higher torus spread. On the other hand, as absorption increases, the parameter combinations span fewer and fewer objects at a time. This is because, as the universally mildly absorbed power-law is attenuated, the interesting physics of the complex absorbing material emerges, revealing each source to be unique.

This methodology will be applied to an expanded sample and the resulting maximally spanning sets of model parameter combinations will be used to simulate AGN observations with Athena. These simulations will then be used to test and develop our automated method to extract spectroscopic redshifts from X-ray AGN spectra.

Acknowledgments

Activities partially funded by project RTI2018-096686-B-C21 funded by MCIN/AEI/10.13039/501100011033 and by "ERDF A way of making Europe" and by the Agencia Estatal de Investigación, Unidad de Excelencia María de Maeztu, ref. MDM-2017-0765.

References

- [1] Brandt WN, Alexander DM. 2015, *Astron Astrophys Rev*, 23(1):1
- [2] Buchner J, Brightman M, Nandra K, Nikutta R, Bauer FE. 2019, *A&A*, 629:A16
- [3] Castelló-Mor N, Barcons X, Ballo L., 2011, *Advances in Space Research*, 48(7):1304–10
- [4] Ceraj L, Smolčić V, Delvecchio I, Novak M, Zamorani G, et al, 2018, *A&A*, 620:A192
- [5] Civano F, Cappelluti N, Hickox R, Canning R, Aird J, et al, 2019, *Bulletin of the AAS*, 51(3):
- [6] Corral A, Della Ceca R, Caccianiga A, Severgnini P, Brunner H, et al., 2011, *A&A*. 530:A42
- [7] Wilkins DR, Fabian AC. 2011, *MNRAS*, 414(2):1269–77
- [8] Elitzur M., 2006, *New Astronomy Reviews*, 50(9–10):728–31
- [9] Fabian, A. C., Iwasawa, K., Reynolds, C. S., Young, A. J. *PASP*, 2000, 112, 1145
- [10] Fanidakis N, Baugh CM, Benson AJ, Bower RG, Cole S, et al. 2012, *MNRAS*, 419(4):2797–2820
- [11] Fiore F, Puccetti S, Grazian A, Menci N, Shankar F, et al, 2012, *A&A*, 537:A16
- [12] Haardt F. and Maraschi L., 1993, *ApJ*, 413:507
- [13] Ghosh R, Laha S. 2021. *ApJ*. 908(2):198
- [14] Harrison, F. A., Craig, W. W., Christensen, F. E., et al. 2013, *ApJ*, 770, 103
- [15] Heckman TM, Best PN, 2014, *Annu. Rev. Astron. Astrophys*, 52(1):589–660
- [16] Krolik JH, Begelman MC, 1988, *ApJ*, 329:702
- [17] Lanzuisi G, Delvecchio I, Berta S, Brusa M, Comastri A, et al. 2017, *A&A*, 602:A123
- [18] Markowitz AG, Krumpke M, Nikutta R. 2014, *MNRAS*, 439(2):1403–58
- [19] Nenkova M, Ivezić Ž, Elitzur M. 2002. *ApJ*. 570(1):L9
- [20] Netzer H, 2013, Cambridge University Press, 353 pp.
- [21] Padovani P, 2017, *Front. Astron. Space Sci.* 4:35
- [22] Sicilian D, Civano F, Cappelluti N, Buchner J, Peca A, 2022, *ApJ*, 936(1):39
- [23] Simmonds C, Buchner J, Salvato M, Hsu L-T, Bauer FE, 2018, *A&A*, 618:A66
- [24] Wang F, Yang J, Fan X, Hennawi JF, Barth AJ, et al, 2021, *ApJL*, 907(1):L1